Pyrometric measurement of the temperature of shocked molybdenum

A. Seifter*
Los Alamos National Laboratory, Los Alamos, New Mexico 87545, USA

D. C. Swift
Lawrence Livermore National Laboratory, Livermore, California 94550, USA

(Received 16 December 2007; revised manuscript received 2 March 2008; published 8 April 2008)

Measurements of the temperature of Mo shocked to ~60 GPa and then released to ~28 GPa were previously attempted by using high explosive driven flyer plates and pyrometry. The analysis of the radiance traces at different wavelengths indicates that the temporal evolution of the radiance can be explained by a contribution from the LiF window to the measured thermal radiation. By fitting the radiance traces with a simple model, which is supported by continuum dynamics studies, which were able to relate structures in the radiance history to hydrodynamic events in the experiment, the contribution of the window, and hence the temperature of the Mo sample, was obtained. The shock and release temperature obtained in the Mo was 762 ± 40 K, which is consistent with calculations taking the contribution of plastic work to the heating into account. The radiance obtained for the LiF window shows a nonthermal distribution that can be described by a bulk temperature of 624 ± 112 K and hot spots (less than 0.5% in total volume) within the window at a temperature of about 2000 K.

DOI: 10.1103/PhysRevB.77.134104 PACS number(s): 62.50.Ef, 07.20.Ka

I. INTRODUCTION

The measurement of temperature in shock physics experiments is of paramount importance since temperature is required as a constraint (in addition to pressure and volume) for the development and credibility of robust multiphase equations of states (EOSs). The application of modern material strength models requires these EOSs with accurate temperatures and phase boundaries, particularly melt curves. Temperature is an important parameter in geophysics and planetary sciences for an accurate description of planetary structures and astrophysical impacts. Many measurements of the EOSs of planetary materials and the pressure calibration on which diamond anvil cell studies rely are made by using shock experiments and rely on temperature corrections to infer states off the shock Hugoniot. General research and model development for the response of materials to extreme dynamic conditions focuses on multiscale approaches, in which physics-based models (as opposed to empirical relations) for thermally activated processes including plastic flow, phase changes, and chemical reactions require an accurate knowledge of the temperature. As a specific example, the melting curve and kinetics of beryllium and carbon (diamond) at elevated pressures are important to understand the behavior of ablator capsules for the National Ignition Facility to succeed in harvesting fusion energy from laser driven capsule implosions.[1]

Pyrometry is a form of thermal emission spectrometry in which the emission spectrum is collected in a small number of spectral bands with significant bandwidth compared to energy-dispersive spectrometers such as prisms and gratings. Energy-dispersive spectrometers are not practical for most shock experiments at temperatures below a few thousand Kelvin because the thermal emission is too weak to take advantage of the relatively fine spectral resolution. Pyrometry is thus the most promising technique applicable to many materials and experimental configurations [besides neutron resonance spectroscopy[2,3] (NRS) and Raman spectroscopy,[4] both with their advantages and limitations] to achieve the goals stated above. Nevertheless, although pyrometry has been fielded on dynamic loading experiments for more than four decades,[5] it still suffers from problems such as background light, thermal and nonthermal emissions from the window material, and sample/window interface effects, which are hard to take into account.

NRS has been investigated as a possible bulk-temperature diagnostic for shock physics experiments because it is capable of measuring the temperature within opaque samples. Initial experiments on shock loaded Mo showed significant discrepancy with theoretical predictions. To investigate this discrepancy, microsecond-duration pyrometric measurements were performed on Mo samples through LiF windows. These experiments used the same shock generation method that was used in the NRS experiments and also included Doppler velocimetry measurements of the surface velocity history of the sample to verify the loading conditions. Previous analysis of the pyrometry experiments[6] did not succeed in extracting temperatures. Here, we report a more rigorous study of the effects of shock and release waves on pyrometry measurements with a release window, identifying a two-temperature population from pyrometry data. We are able to correlate features of the radiance history at a level usually dismissed as too complicated for further analysis and provide valuable insight into the dynamic processes occurring in shock experiments using a window. This allows us to extract temperatures more accurately and with greater confidence. The results presented the simultaneous extraction of sample and window temperatures, which enhances the ability to reliably interpret pyrometry data. This study is key to future research and physics-based understanding of the response of condensed matter subject to dynamic loading and heating.

II. EXPERIMENTAL SETUP

As in the NRS experiments, a shock was induced in the Mo sample by the impact of an Al disk accelerated to a speed of about 3.5 km/s by means of high explosive (HE) gases.[7] A LiF window was glued to the back side of the Mo disk (where the measurement was made) to maintain a high pressure over an area accessible for contactless temperature measurements.[8] The emitted thermal radiation was focused onto a 1 mm core-diameter near-infrared (NIR) fiber as well as onto a 1 mm core-diameter visible-glass, low OH fiber. Two different multichannel pyrometers with different spectral responses were used to infer thermal radiance over a wide range of wavelengths: a visible pyrometer with five channels in the visible and NIR wavelength regions by using photomultiplier tubes (PMTs) and an IR pyrometer with four channels in the NIR by using InSb detectors. The velocity history at the Mo/LiF interface was measured by laser Doppler velocimetry, using a velocity interferometer system for any reflector[9] (VISAR), to infer the pressure history applied to the sample.

In the case of low-temperature pyrometry measurements, special precautions have to be taken in order to avoid background light, which can easily overwhelm especially the short wavelength channels. These backgrounds can be generated either by bright HE gases blowing by the target, air lighting up due to shock luminescence from nitrogen, ejecta or jets generated due to improper surface preparation, or sharp edges. In order to minimize the background, the experiments were performed in a vacuum (10^{-3} Torr). Two CaF_2 lenses were used to focus the thermally emitted light onto a 1 mm diameter NIR fiber[10] (centered 2.5 mm off axis at the fiber bundle) and a 1 mm diameter visible low OH fiber[11] (centered 2.5 mm diametrically opposed). The center fiber was a VISAR probe[12] used to determine the velocity of the sample after impact. Figure 1 shows a sketch of the experimental setup. The LiF window was included to maintain an elevated pressure in the Mo when the shock reached its surface, avoiding release to atmospheric pressure. The LiF was attached to the Mo coupon using Loctite® 326 glue, which has been previously found[13] to not cause considerable amounts of thermal emission. This simplifies the relating of the surface temperature to the bulk temperature of the shocked sample. However, thermal light emission from both the glue layer and the LiF is a concern.

The IR pyrometer collimates and divides the incoming light from a single NIR fiber into four spectral ranges by using three custom dichroic beam splitters. These four collimated beams are spectrally narrowed by bandpass filters centered at 1.8, 2.3, 3.5, and 4.8 μm and then refocused onto the 1 mm^2 active area of the 50 MHz bandwidth InSb detectors by using ZnSe lenses. The lower temperature limit of the two longer wavelength channels is about 340 K (by assuming an emittance of 1). For more information on the NIR instrument and on data analysis, see Ref. 14.

The visible pyrometer also uses dichroic beam splitters to spectrally divide the incoming light into five beams, which are then refocused onto the active area of the PMTs. Also by using bandpass filters, these five channels are centered at 505 nm, 725 nm, 850 nm, 1.23 μm, and 1.59 μm. A holographic notch filter is used to suppress the bright 532 nm laser light used for the VISAR measurements. More information on this instrument can be found in Ref. 15.

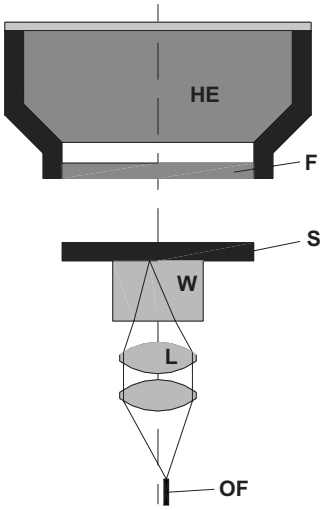

FIG. 1. Schematic setup of the experiment. S, molybdenum sample (⌀64×6 mm); *W*, LiF window (⌀30×20 mm), F; aluminum flyer (⌀64×5 mm, 20 mm gap between F and S); HE, 9501 high explosive (7 mm gap between HE and F); L, CaF_2 lenses (⌀25 mm, f=50 mm); OF, optical fibers (⌀1 mm C2 fiber, ⌀1 mm low OH fiber and VISAR fiber bundle).

For further details on the HE-driven flyer system, see Refs. 7 and 16.

III. RESULTS

Eight experiments have been performed at the "Chamber-8" high explosive experimental facility at the Los Alamos National Laboratory in September 2004; these experiments are summarized in Table I.

Figure 2 shows the radiance as a function of time as well as the sample/window interface velocity for experiment 06. The time of shock breakout is set to t=0 μs. If no unwanted background light occurs, then the radiances are expected to be constant from the time of shock breakout until the released wave from the back of the flyer reaches the sample/

TABLE I. Experiments performed. Surface condition (free surface or window) and diagnostics (V, VISAR; IR, IR pyrometer; vis, visiblepyrometer).

Expt. No.	Surface	Diagnostics	Comments
01	LiF window	V, IR	Data clipped
02	LiF window	V, IR	Data lost
03	LiF window	V, IR	Good data
04	Free surface	V, IR	HE problems, no data
05	Free surface	V, IR	Good data
06	LiF window	V, IR, vis	Good data
07	LiF window	V, IR, vis	Good data
08	Free surface	V, IR, vis	Good data

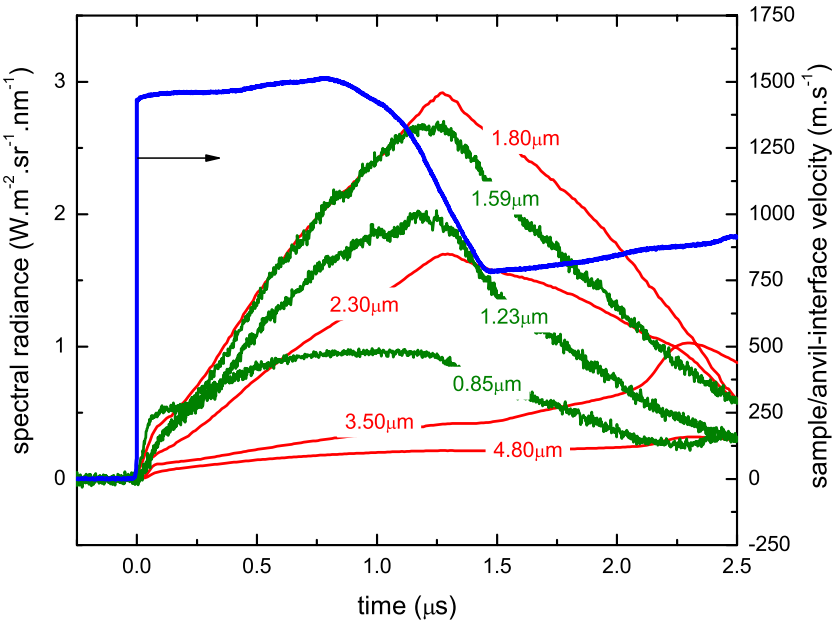

FIG. 2. (Color online) Measured radiances for seven wavelengths (red, IR pyrometer; green, visible/NIR pyrometer) and sample/window interface velocity (blue) for experiment 06.

window interface (about 0.7 μs after breakout). At this time, the sample/window interface decelerates to a lower velocity, as can be seen from the particle velocity trace.

Continuum dynamics simulations were used to investigate the origin of the varying signals in the shocked state by comparing them to the various hydrodynamic events occurring in the experiments. One dimensional (1D) and two dimensional (2D) simulations were performed by using general-purpose multiphysics hydrocodes. Shock dynamics calculations were also performed using the same material properties by solving the Rankine–Hugoniot equations to obtain shock states, and hence wave speeds, more precisely than by derivation from the discretized hydrocode solutions.[17] The 1D and 2D hydrocodes both used a finite difference representation of spatial fields, a second-order predictor-corrector algorithm for time integration, and an artificial viscosity to stabilize the shocks. The 1D simulations, which are along the axis of symmetry, were Lagrangian, avoiding inaccuracies caused by numerical advection, and used the LAGC1D hydrocode.[18] The 2D simulations, which are axisymmetric in the axial-radial plane, were Eulerian, making them robust in treating a highly distorted flow from sharp corners, with an operator-split third-order van Leer flux limited method for advection, and used the EUL2D hydrocode.[19]

The simulations included the HE-driven flyer, the Mo target, and the LiF window. The HE acceleration system itself was not modeled: the flyer was treated as flat and moving at a constant speed starting from the instant of impact. In reality, the flyers were slightly dished, still accelerating slightly, and reverberating, but these details should not make a significant difference to the pyrometry data. The EOSs used the cubic Grüneisen form with published parameters for each material.[20] Some simulations were repeated using EOSs from the SESAME tabular compendium;[21] the difference was negligible. Strength was treated using the Steinberg–Guinan model,[22] with published parameters for each material.[20] In the 1D simulations, the cell sizes in the flyer, sample, and window were 0.1, 0.05, and 0.2 mm, respectively. In the 2D simulations, the cell size was 0.1 mm.

A position-time diagram for the key mechanical waves from the 1D simulations is shown in Fig. 3 (lower part) together with the measured spectral radiance at 2.3 μm for experiment 06.

The radiance increased from the time of shock breakout until about 2.1 μs. Then, the radiance decreased at a rate slightly lower than that of the increase. The kink in the radiance at about 3.1 μs occurs at about the time when the release from the edge of the window reaches the center of the sample/window interface, cooling it by adiabatic expansion. The shock wave reaches the rear surface of the window at about 3.75 μs. At this time; the signal of all the wavelengths goes into saturation because of a bright flash that occurs at this event.

The recorded pyrometer output signals for experiment 01 have been clipped because the settings of the digitizer have been too sensitive (the increase in radiance with time was not expected). The measured radiances for the other successful experiments look very similar to the ones shown in Fig. 2 (for experiment 06) and are not shown here.

The radiance traces for the free surface experiments are not analyzed and discussed here because, in addition to problems with background light, the surface temperature was not homogeneous. (This can be inferred from the response of the different wavelengths shortly after the time of shock breakout. For more details on spatial temperature nonuniformities, see Ref. 23.) The background light at the free surface experiments was most likely caused by thermal radiation from APIEZON Q©, which is a soft, black, puttylike substance that was intended to absorb the thermal radiation from the hot jets formed at the edge of the sample/window interface.

IV. DATA ANALYSIS

Figure 4 shows the parts involved in the process of emission of thermal light for the sample/window combination

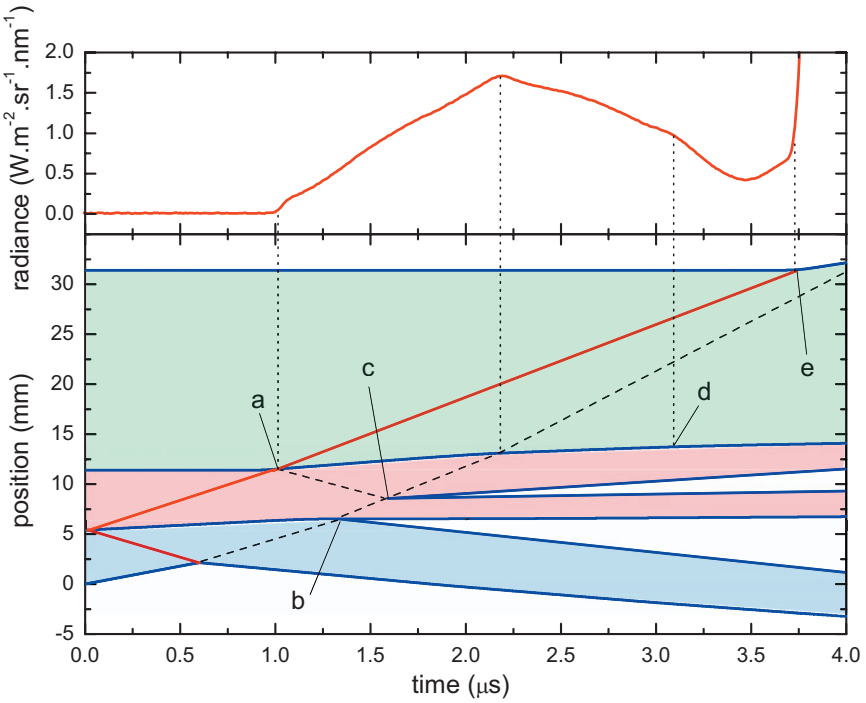

FIG. 3. (Color) x-t diagram [lower part: blue lines, boundaries between flyer (blue), sample (red), and window (green); red lines, shock front; dashed lines, release waves (mean velocity)] and measured spectral radiance at 2.3 μm for experiment 06 (upper part: the time has been shifted so that the breakout at the sample/window interface occurs at the same time as that at the simulated x-t diagram). The events labeled in the lower part are as follows: (a) shock reaches the sample/window interface; (b) flyer bounces off the sample when the release wave reaches the interface; (c) release waves from the back of the flyer and the sample/window interface meet inside the sample and cause the sample to spall; (d) edge release waves reach the symmetry axis of the experiment (the radial effect does not correspond to the events in the 1D axial wave diagram); (e) shock wave reaches the free surface of the window.

used in these experiments, including the effect of the interface between the shocked and unshocked window materials.

The thermal emitted radiance from the sample (L_{sample}) is multiply reflected between the interfaces R_1, R_2, and R_3. These reflectivities can be obtained from the optical properties of the sample and the shocked and the unshocked window. The index of refraction of the shocked window can be estimated from the Gladstone–Dale relation.[24] From this, it can be seen that R_2 is very small and can be neglected.[25] The index of refraction and extinction coefficient of the unshocked window can be found in Ref. 26. The absorption in this part can be neglected as well. The shocked part of the window can emit thermal radiation (L_{window}) as well as absorb the thermal radiation emitted by the sample. The emissive power of translucent materials (equivalent to the emissivity of opaque materials) can be expressed by $(1-e^{-\alpha x})$, and the absorption can be expressed by $e^{-\alpha x}$, where x is the thickness of the shocked layer and α is the absorption coefficient.[27] The absorption coefficient is related to the extinction coefficient by the following relation:

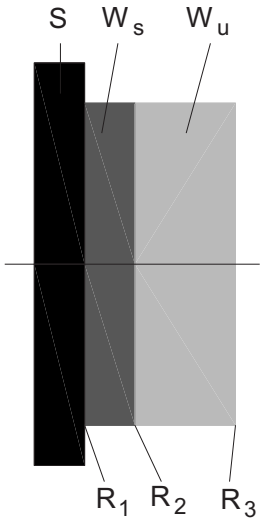

FIG. 4. Schematic of the window/sample combination. S, sample; W_s, shocked window; W_u, unshocked window; R_{1-3}, interface reflectivities.

$$\alpha = \frac{4\pi k}{\lambda_0}, \tag{1}$$

where k is the extinction coefficient and λ_0 is the wavelength in vacuum. Thus, the radiance from this assembly can be expressed as

$$L = \frac{(1-R_3)}{(1-R_1R_3e^{-2\alpha x})}[L_{\text{sample}}\tilde{\epsilon}e^{-\alpha x} + L_{\text{window}}(1+R_1e^{-\alpha x})(1-e^{-\alpha x})], \tag{2}$$

where $\tilde{\epsilon}$ is the effective emissivity of the sample into the window, taking the interface effects and absorption of the

TABLE II. Fitting results for experiments 01, 03, 06, and 07. Where there are no data available (due to low signal level or poor quality of the fit), the cells have been left blank.

Expt. No.	λ (μm)	ϵL_{Mo} (W/m^2 nm sr)	L_{LiF} (W/m^2 nm sr)	a_{LiF} (mm^{-1})
01	3.5	0.117	2.27	0.0109
	4.8	0.051	0.229	0.0988
03	3.5	0.110		
	4.8	0.062		
06	0.85			0.38694
	1.23		16.3	0.11307
	1.59		15.8	0.08272
	1.8	0.072	4.73273	0.0472
	2.3	0.088	3.2168	0.0239
	3.5	0.06401	0.85708	0.03602
07	4.8	0.02808	0.45	0.11792
	1.23	0.004		
	1.59	0.025		
	1.8	0.102		
	2.3	0.108		
	3.5	0.132		
	4.8	0.069		0.1234

glue layer into account. The emissivity is mainly determined by the optical properties (n and k) of the sample and the window but can increase if the interface roughness increases following shock breakout, for instance, if the interface is Richtmyer–Meshkov unstable or because of flow or jetting from the surface texture.

The first term in Eq. (2), $(1-R_3)/(1-R_1R_3e^{-2\alpha x})$, is very close to 1 (between 0.98 and 1.0 in all practical cases) and can be set to 1 without compromising the accuracy of the analysis. The term $(1+R_1e^{-\alpha x})(1-e^{-\alpha x})$ can be simplified to $(1-e^{-2\alpha x})$ without compromising the fitting results for the sample radiance, introducing an error in the window radiation and absorption coefficient of less than 10%, which is far below the uncertainty of the fitting parameters. Thus, Eq. (2) can be approximated as

$$L = L_{\mathrm{sample}}\tilde{\epsilon}e^{-\alpha x} + L_{\mathrm{window}}(1 - e^{-2\alpha x}). \tag{3}$$

The thickness x of the shocked layer is given by $x=(u_s-u_p)t$, where u_s is the shock velocity in LiF (7.10 mm/μs at a pressure of 27 GPa) and u_p is the particle velocity at the sample/window interface (1.45 mm/μs on release into LiF from a Hugoniot pressure of 64 GPa in molybdenum) and t is the time after shock breakout at the Mo/LiF interface. Equation (3) was used to fit the radiance traces of experiments 01, 03, 06, and 07. The results are shown in Table II.

While the emissive power of the window material[27] was obtained from the fitting parameters, and hence the temperature of the shocked window can be directly obtained, the inferred temperature of the sample strongly depends on the effective emissivity $\tilde{\epsilon}$ of the sample/window combination. Since this property is very hard to experimentally determine, it is common practice to assume lower and upper emissivity bounds and use these bounds to calculate the upper and lower bounds for the temperature.[28] This has been done for experiments 06 and 07 (where a sample radiance L_{sample} was obtained) with the following lower ϵ_l and upper ϵ_u emissivity bounds: $\lambda=1.23$ μm: $\epsilon_l=0.2$, $\epsilon_u=1.0$; $\lambda=1.59$ μm: $\epsilon_l=0.15$, $\epsilon_u=0.8$; $\lambda=1.80$ μm: $\epsilon_l=0.12$, $\epsilon_u=0.8$; $\lambda=2.30$ μm: $\epsilon_l=0.1$, $\epsilon_u=0.6$; $\lambda=3.50$ μm: $\epsilon_l=0.08$, $\epsilon_u=0.4$; $\lambda=4.80$ μm: $\epsilon_l=0.05$, $\epsilon_u=0.3$. These estimates are based on the room temperature values (which were obtained from the optical properties) for polished surfaces[26,29] and the melting temperature values at ambient pressures.[28] The calculated true sample temperature bounds for experiments 06 and 07 as a function of wavelength are shown in Fig. 5 (for readability reasons, the wavelengths for experiment 06 have been shifted by 0.1 μm to the red).

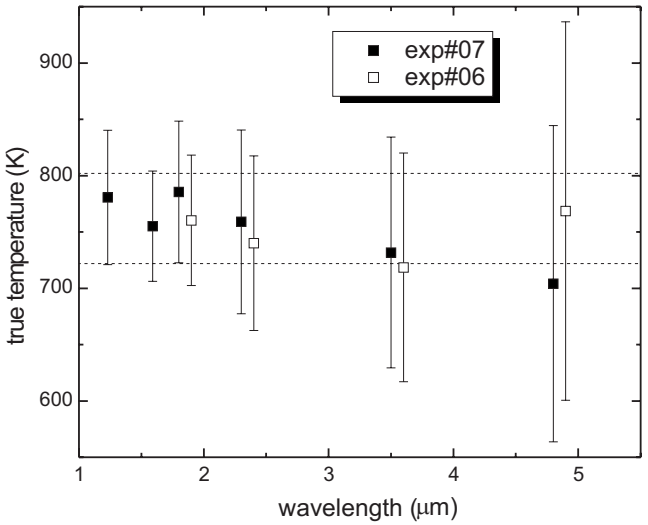

FIG. 5. Upper and lower bounds for sample temperature as a function of wavelength for experiments 06 and 07 (the wavelengths for experiment 06 have been shifted by 0.1 μm to the red for readability reasons).

It can be seen that the uncertainty due to unknown emissivity increases with increasing wavelength. This is due to the fact that the relative change in radiance for a given change in temperature decreases with increasing wavelength, and hence, a given uncertainty in radiance (e.g., due to unknown emissivity) results in a smaller uncertainty in temperature at shorter wavelengths. (A more detailed explanation can be found in Ref. 23.) The temperature ranges for all wavelengths overlap between 722 and 802 K; this is the range where the temperature of the sample shocked to a Hugoniot pressure of 63.9 ± 2.4 GPa and released into LiF (at an interface pressure of 27.1 ± 1.0 GPa) is determined. The Hugoniot pressures in the sample have been obtained from the measured particle velocity at the sample/window interface. The pressures in the LiF window have been obtained from jump conditions and known shock properties of the window material through the published EOSs and strength model.[20]

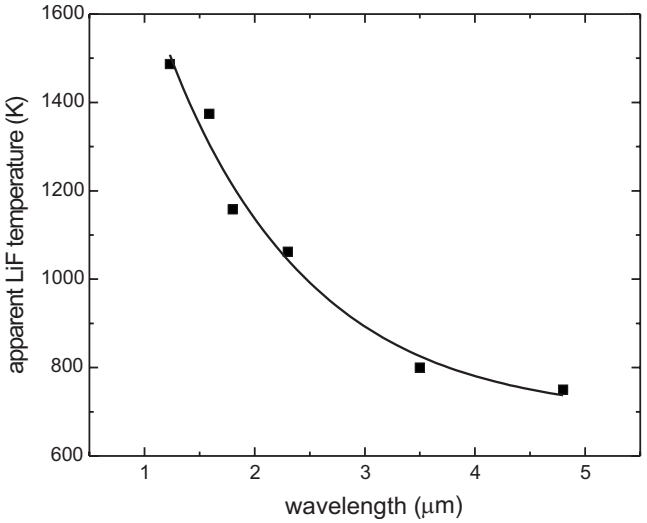

FIG. 6. Apparent window temperature as a function of wavelength (squares) from experiment 06. The solid line is the result from fitting the measured data with a simple two-temperature model (Ref. 23). The results of the fitting process are presented in the text below.

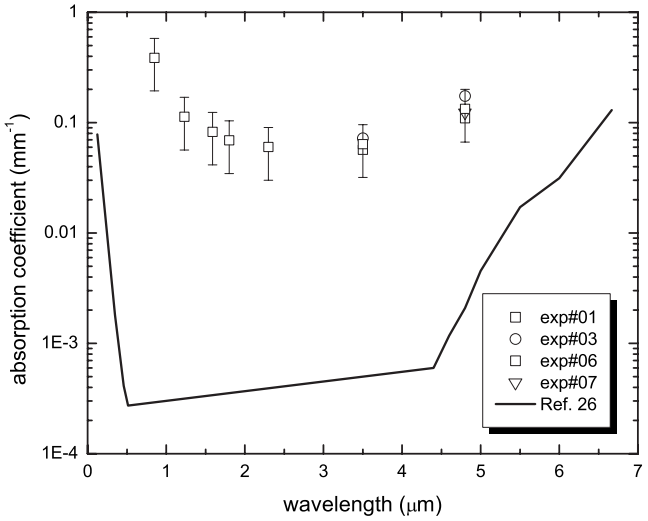

FIG. 7. Absorption coefficient for shocked LiF (27.1 ± 1.0 GPa) as a function of wavelength for all of the wavelengths and experiments where these data could be obtained from the fitting process. The solid line shows literature values for LiF at standard conditions.

The temperature of the LiF window as a function of wavelength from experiment 06 is shown in Fig. 6.

If the window is at a homogeneous temperature and no background light occurs, the measured window temperature should be independent of wavelength. The increase in the measured window temperature (apparent temperature) with decreasing wavelength indicates a nonhomogeneous window temperature. Fitting the results with a simple two-temperature model (for details, see Ref. 23) gives a temperature of 624 ± 112 K for the window with hot cells at a temperature of 1945 ± 210 K. The area fraction (as seen from the pyrometer) of these hot cells was determined to be 3.0 +(1.5%), corresponding to a volume fraction of less than 0.5%. The absorption coefficient as a function of wavelength for the shocked LiF window is shown in Fig. 7. The solid line shows data from Ref. 26 at room temperature and ambient pressure. It can be seen that the absorption coefficient increases by roughly 2 orders of magnitude compared to the literature data independent of wavelength.

It can be seen from Fig. 3 that the radiance increases as long as the thickness of the shocked layer in LiF increases (from shock breakout at the Mo/LiF interface at 1.0 μs until the released wave from the back of the aluminum flyer reaches this interface at about 2.1 μs). The thickness of the shocked LiF layer decreases after $t=2.1$ μs because the released wave propagates at a higher velocity than that of the shock wave, and hence, the measured radiation decreases between $t=2.1$ μs and about 3.7 μs. At 3.7 μs, the shock front in the LiF reaches the free surface of the window, and the measured radiance abruptly increases, which is assumed to be due to nonthermal light emission when the window fractures on release from the shocked state and the air shock.[30]

From fitting the spectral radiance traces at different wavelengths and assuming lower and upper bounds for the effective emissivity of the sample/window assembly, a sample temperature (shocked to 63.9 ± 2.4 GPa and released to a pressure of 27.1 ± 1.0 GPa into LiF) at the interface of 762 ± 40 K could be obtained. Since the temperature readings of different wavelength channels agree (see Fig. 5), it can be concluded that the temperature is spatially uniform, and hence, hot spots due to shear bands or other reasons do not occur.[23] The release temperature into LiF was calculated to be 670 ± 25 K by using the Steinberg–Guinan strength model to predict the contribution to heating from plastic work.[31] The resulting temperatures are in relatively good agreement[32] with experiments performed on a gas gun at a slightly lower pressure ($T=683 \pm 41$ K at a Hugoniot pressure of 58.7 GPa, with a release pressure of 24.8 GPa into LiF). A summary of all the experimental and calculated results can be seen in Fig. 8.

The measured temperature in the LiF window is 624 ± 112 K with hot spots [3.0($\pm$1.5%) in area] with a temperature of 1945 ± 210 K. These hot spots are believed to occur due to the slightly nonuniaxial loading of the sample and window[3] due to the dishing of the flyer plate, which most likely causes local heating by shear strain localization. This localized heating in LiF windows was also observed in infrared imaging experiments.[33] The temperature of the LiF window was calculated to be 569 ± 15 K,[31] which is in excellent agreement with the temperature inferred from the experiment. An analysis of the free surface experiments was not possible because of temperature nonuniformities combined with background light caused by the hot APIEZON Q© (which is used to block thermal emission from the hot jets from the edges, as was discussed above).

V. CONCLUSIONS

Reliable pyrometric temperatures were obtained at shocked and released surfaces despite an $O(100\%)$ back-

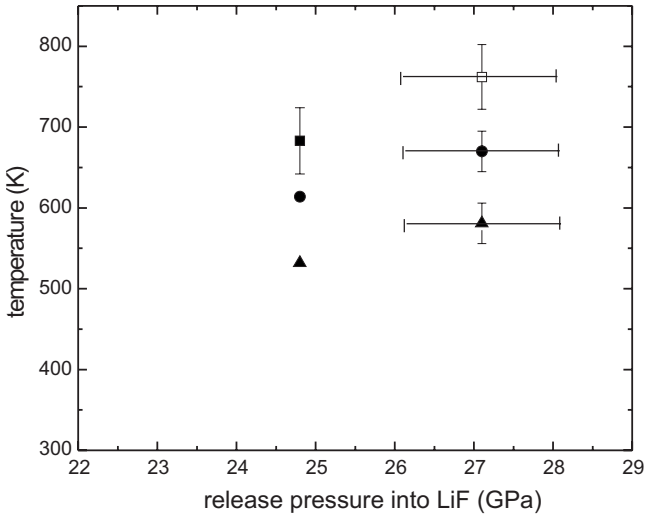

FIG. 8. Measured and calculated temperatures for molybdenum released into LiF for two different release pressures. Open square, this experiment; full square, gas gun experiment (Ref. 31); circles, calculations taking strength into account via the Steinberg–Guinan model (Ref. 22); triangles, calculations ignoring strength effects (Ref. 22).

ground from shocked window material. This improvement was achieved by using the emission spectrum to infer a volume fraction of hot spots in the window and was supported by relating changes in the emitted radiance to predictions of hydrodynamic events in the window. The measured temperature for Mo at a Hugoniot pressure of 63.9 ± 2.4 GPa released into LiF to an interface pressure of 27.1 ± 1.0 GPa of 762 ± 40 K is in good agreement with temperatures measured by using a powder gun at a slightly lower pressure (58.7 GPa released to 24.8 GPa) of 683 ± 41 K. The measured temperatures are slightly higher than those from calculations using the Steinberg–Guinan model[22] to take strength effects into account. It is not clear whether the remaining discrepancy is caused by additional sources of thermal emission not taken into account or inaccuracy in the models used in the simulations. However, this level of agreement is unusually good for thermal emission from shocked metals.

Besides the release temperature of Mo, the shock temperature of LiF at a pressure of 27.1 ± 1.0 GPa was also obtained and is in good agreement with calculations. The shock temperature in the window was much less sensitive to the strength model.

Because of problems in controlling the thermal background, free surface temperatures could not be extracted from the experiments without a window.

ACKNOWLEDGMENTS

The work was performed under the auspices of the U.S. Department of Energy under Contract Nos. W-7405-ENG-36 and DE-AC52-06NA25396.

*Corresponding author; seif@lanl.gov

[1] Y. M. Gupta (unpublished).
[2] V. W. Yuan, J. D. Bowman, D. J. Funk, G. L. Morgan, R. L. Rabie, C. E. Ragan, J. P. Quintana, and H. L. Stacy, Phys. Rev. Lett. **94**, 125504 (2005).
[3] D. C. Swift, A. Seifter, D. B. Holtkamp, V. W. Yuan, D. Bowman, and D. A. Clark, Phys. Rev. B **77**, 092102 (2008).
[4] R. L. Gustavsen and Y. M. Gupta, J. Appl. Phys. **75**, 2837 (1994).
[5] S. B. Kormer, M. V. Sinitsyn, G. A. Kirilliv, and V. D. Urlin, Sov. Phys. JETP **21**, 689 (1965).
[6] A. Seifter, K. Boboridis, D. A. Clark, R. B. Corrow, D. B. Holtkamp, C. W. McCLuskey, G. L. Morgan, J. R. Payton, P. Quintana, C. E. Ragan, P. Rodriguez, H. L. Stacy, W. S. Vogan, V. W. Yuan, and A. W. Obst, in *Proceedings of the Ninth International Symposium on Temperature Measurements in Industry and Science (TEMPMEKO)*, edited by D. Zvizdic, L. G. Bermanec, T. Veliki, and T. Stasic (Laboratory for Process Measurement, Faculty of Mechanical Engineering and Naval Architecture, Zagreb, Croatia, 2004), Vol. 2, p. 1185.
[7] C. A. Forest, J. Vorthman, L. Bennet, and R. L. Rabie, Los Alamos National Laboratory Technical Report No. LA-UR-98-3783, 1998 (unpublished).
[8] J. R. Asay and M. Shahinpoor, *High-Pressure Shock Compression of Solids* (Springer, New York, 1992), pp. 32–34.
[9] L. M. Barker and R. E. Hollenbach, J. Appl. Phys. **43**, 4669 (1972).
[10] Chalcogenide glass fiber (C2) from Amorphous Materials Inc., Garland, TX, (www.amorphousmaterials.com).
[11] Polymicro Technologies, Phoenix, AZ (www.polymicro.com).
[12] One injection fiber in the center surrounded by seven receiving fibers each 100 μm in diameter.
[13] P. L. Hereil and C. Mabire, J. Phys. IV **10**, Pr9–749 (2000).
[14] A. Seifter, K. Boboridis, J. R. Payton, and A. W. Obst, in *Proceedings of the 26th International Congress on High-Speed Photography and Photonics*, edited by D. L. Paisley, S. Kleinfelder, D. R. Snyder, and B. J. Thompson (Los Alamos National Laboratory, Los Alamos, NM, 2005), Vol. 5580, pp. 93–105.
[15] D. B. Holtkamp (unpublished).
[16] D. C. Swift, C. A. Forest, D. A. Clark, W. T. Buttler, M. Marr-Lyon, and P. Rightley, Rev. Sci. Instrum. **78**, 063904 (2007).
[17] D. C. Swift, Los Alamos National Laboratory Report No. LA-UR-07-2051, 2007 (unpublished).
[18] *Program and Manuals for lagc1d Program* (Wessex Scientific, Perth, 2006).
[19] *Program and Manuals for eul2d Program* (Wessex Scientific, Perth, 2006).
[20] D. J. Steinberg, Lawrence Livermore National Laboratory Technical Report No. UCRL-MA-106439, 1996 (unpublished).
[21] K. S. Holian, Los Alamos National Laboratory Technical Report No LA-10160-MS-v.1C, 1984 (unpublished).
[22] D. J. Steinberg, S. G. Cochran, and M. W. Guinan, J. Appl. Phys. **51**, 1498 (1980).
[23] A. Seifter and A. W. Obst, Int. J. Thermophys. **28**, 934 (2007).

[24] J. H. Gladstone and T. P. Dale, Philos. Trans. R. Soc. London **153**, 317 (1863).

[25] At a pressure of 200 kbar in the anvil, the reflectivity R_2 is less than 0.1%. It increases to 0.25% at 500 kbar and to 0.5% at 1 Mbar.

[26] E. D. Palik, *Handbook of Optical Constants of Solids* (Academic, New York, 1990).

[27] R. Gardon, J. Am. Ceram. Soc. **39**, 278 (1956).

[28] V. Vujnovic and B. Grzeta, Fizika (Zagreb) **4**, 173 (1972).

[29] The normal spectral emissivity for a flat surface is obtained by $\varepsilon_\perp = \frac{4n_1n_2}{(n_1+n_2)^2+k_2^2}$, with n_1 and n_2 the indices of refraction of the anvil and the sample, respectively, and k_2 is the extinction coefficient of the sample.

[30] The 10^{-3} Torr vacuum is intended to provide the same experimental conditions as for the NRS experiments (avoiding drag forces on the Al flyer plate). This vacuum is not low enough to prevent bright emissions from the shocked air.

[31] D. C. Swift, A. Seifter, D. B. Holtkamp, and D. A. Clark, Phys. Rev. B **76**, 054122 (2007).

[32] For both calculations (with and without strength), the temperature at 24.8 GPa is about 55 K lower than that at 27.1 GPa. The measured data point at 24.8 GPa is 79 ± 35 K lower than that at 27.1 GPa.

[33] M. D. Wilke, 2007 (private communication).